JOURNAL OF GEOPHYSICAL RESEARCH, VOL. 103, NO. D1, PAGES 1405–1415, JANUARY 20, 1998

Factors influencing the retention of hydrogen peroxide and molecular oxygen in rime ice

Jefferson R. Snider and Jun Huang

Department of Atmospheric Science, University of Wyoming, Laramie

Abstract. Vertical transport of many atmospheric trace gases is modulated by retention in solid (ice phase) precipitation during the impaction and freezing (i.e., riming) of supercooled cloud droplets. Here we report field measurements of the concentrations of both hydrogen peroxide (H_2O_2) and molecular oxygen (O_2) in rime ice. Gas retention efficiencies, defined as the ratio of the observed concentration divided by the equilibrium concentration predicted by Henry's law, are presented. Rime ice collections were conducted in a wind tunnel using 3.2– and 9.5–mm impaction cylinders. Velocities were varied between 9 and 20 m/s and ice substrate temperatures were colder than –3.5 °C. Averaged values of the retention efficiencies for H_2O_2 and O_2 were 0.05 and 0.32, respectively. Also discussed are direct measurements of H_2O_2 volatilization obtained by monitoring increases in gaseous H_2O_2 associated with droplet impingement and freezing on an impaction grid placed upstream of a gas sampling inlet. The observed relationships between retention and the time interval between droplet impaction suggest that H_2O_2 and O_2 are volatilized subsequent to droplet freezing and prior to burial by continued riming. A comparison of the timescales that are expected to govern retention indicates that solute diffusivities in the solidified droplets are ~10^{-12} m^2 s^{-1}.

1. Introduction

Trace gases characterized by large affinities for liquid water are efficiently transferred from the gas to the solution phase during the formation of clouds containing droplets. This is the case for hydrogen peroxide (H_2O_2), formaldehyde and its hydrate, most inorganic and some organic acid vapors, and ammonia. Growing by vapor diffusion, the droplets seldom reach radii larger than 20 μm and frequently exist at temperatures colder than 0°C. Supercooling sets the stage for droplet capture and removal via collision with super–millimetric ice particles (i.e., snowflakes and graupel). During capture the droplets impinge against the surface of falling ice particles and are rapidly frozen. This process results in the retention of some of the dissolved gas. Precipitation resulting from this growth mechanism, commonly referred to as riming, influences the vertical transport of water soluble trace gases [Cho et al., 1989]. In the present article we analyze measurements of the amounts of H_2O_2 and O_2 in rime ice collected from supercooled clouds. These data are used to calculate retention efficiencies expressed as the ratio of the observed concentration in melted rime ice divided by the equilibrium concentration predicted by Henry's law. As in the previous assessments of the retention efficiency, the equilibrium concentration is evaluated at the ambient temperature, not the water ice melting temperature.

Reported values of retention efficiencies for O_2 [Carras and Macklin, 1975], SO_2 [Lamb and Blumenstein, 1987; Iribarne et al., 1990], and H_2O_2 [Iribarne and Pyshnov, 1990; Snider et al., 1992] range between unity and 0.01. Current understanding of the retention process, particularly how retention efficiencies vary with molecular structure of the retained gas and with physical properties of the rime substrate, is lacking. As a result, extrapolations of the limited previous observations to trace gas scavenging by precipitation are associated with considerable uncertainty. In this regard it should be pointed out that the field measurements of Snider et al. [1992] (hereinafter referred to as SMV) yielded substantially lower values for the H_2O_2 retention efficiency than the laboratory studies of Iribarne and Pyshnov [1990]. The reason or reasons for this disparity have not been resolved. SMV suggest that it may stem from the fact that the laboratory experiments were conducted without any ventilation of the rime substrate. There is also concern about the manner in which solute concentrations, in the droplet phase, were inferred from the gas–phase H_2O_2 measurements conducted by SMV.

Many investigators have suggested mechanisms for solute incorporation into ice produced by freezing. There is indirect evidence which indicates that a significant fraction of both N_2 and O_2 can be incorporated into the solid [Bari and Hallett, 1974; Körber, 1988]. Other experiments show that solutes can be entrapped as components of liquid solutions which exist at equilibrium with the solid [Mulvaney et al., 1988]. Since cloud droplets are orders of magnitude smaller than the water systems typically used for investigations of the effect of freezing on solute incorporation into ice, it is expected that additional or different factors may control retention during riming. In recognition of this difference, and based on our analyses of rime ice collected in supercooled clouds, we have hypothesized that H_2O_2 retention is controlled by the rate of rime substrate burial by impinging droplets (SMV).

Here we present field measurements of the concentrations of both O_2 and H_2O_2 in melted rime ice samples. We also compare the derived retention efficiencies to results previously published by SMV. The new measurements were conducted using broader rime

Paper number 97JD02847.
0148-0227/98/97JD-02847$09.00

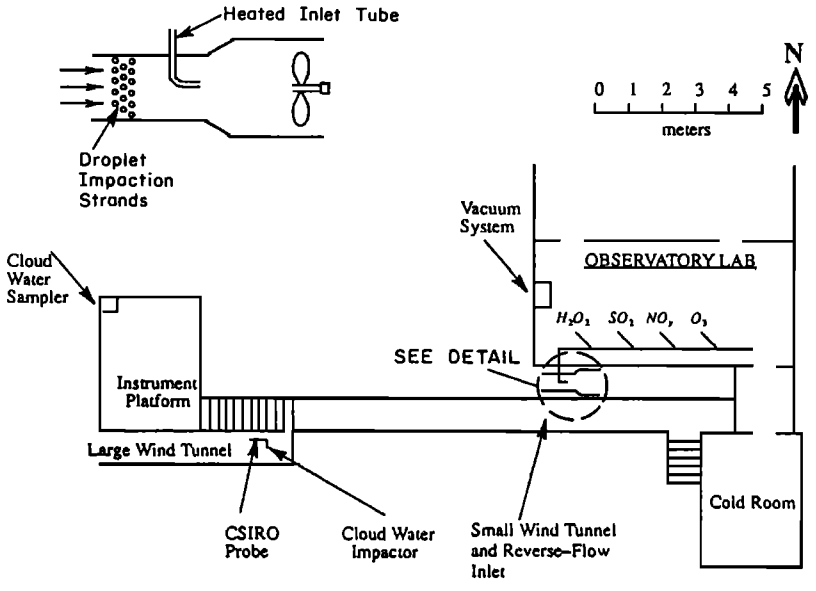

Figure 1. Plan view of Elk Mountain Observatory. The detail drawing shows the small wind tunnel, the heated reverse–flow inlet, and the droplet impaction strands. Only for the experiments discussed in the Appendix were the droplet impaction strands installed.

ice substrates and cover a lower range of droplet impaction velocities. Further, by using a gas–phase monitoring technique we are able to record direct measurements of H_2O_2 volatilization during riming. This technique provides an independent validation of our previous observation that H_2O_2 is not efficiently retained during riming on a ventilated substrate. The new data also reinforce our hypothesis that retention is controlled by the rate of impingement of cloud droplets on the riming substrate.

2. Experiment

2.1. Field Site

Experiments were conducted in supercooled wintertime clouds at the University of Wyoming Elk Mountain Observatory (EMO, 3.3 km above mean sea level, 41°37' N, 106°32' W), located on an isolated peak in southeastern Wyoming, United States. Microphysical characteristics of these clouds are documented by Politovich and Vali [1983]. Droplet growth times are short (<800 s), dispersions (standard deviation of the droplet spectrum divided by the mean radius) are less than 0.3, and the spectra exhibit little or no evidence of broadening due to cloud top entrainment or droplet coalescence. A description of the facility can be found in SMV, and only instrumentation and analytical techniques developed for this study are discussed below. The new instrumentation, shown in Figure 1, consists of the cloud water impactor (CWI) located in the large wind tunnel, the reverse–flow air sample inlet located in the small wind tunnel, and a vacuum system used to process rime ice samples prior to the determination of the amount of retained O_2. Data were collected during three study intervals: (1) March 1991, (2) January 1992, and (3) February 1992.

2.2. Rime Collection and LWC Measurement

In addition to the CWI, which is described in the following paragraph, we used two other devices for measuring cloud liquid water content (LWC). We also employed two of the three instruments for collecting rime ice. Characteristics of these sampling and LWC measuring instruments are summarized in Table 1. Rime ice mass removed from the CWI and from the cloud water sampler (CWS) was used to infer averages of the LWC. In contrast, measurements of the power required to vaporize droplets impinging on the Commonwealth Scientific and Industrial Research (CSIRO) probe [King et al., 1978] was used to infer instantaneous values of the LWC. In section 4 we intercompare H_2O_2 retention values corresponding to rime ice samples obtained from the CWI with retention values obtained using the CWS. The latter measurements were reported in SMV.

The CWI, shown in Figure 2, was used to collect rime ice samples in the large wind tunnel. Tunnel velocities, measured continuously

Table 1. Rime Collection and LWC Measurement Instruments

Device	CWS	CSIRO	CWI	CWI
Width, mm	1.5 [a]	1.8	9.5	3 2
Velocity, m s^{-1}	13 – 24	21	9 – 20	9 – 20
Collision Efficiency, % [b]	69 – 78	75	12 – 28	42 – 60
50% size cut, μm [b]	2.8 – 2.1	2.5	8.8 – 6.2	5.0 – 3.4
Reference	SMV	King et al. [1978]	this work	this work

[a] Average width during a rime collection interval

[b] Calculations based on work of Langmuir and Blodgett [1946], using droplet radius = 4 3 μm, ambient pressure = 670 hPa, and ambient temperature = -10^0C.

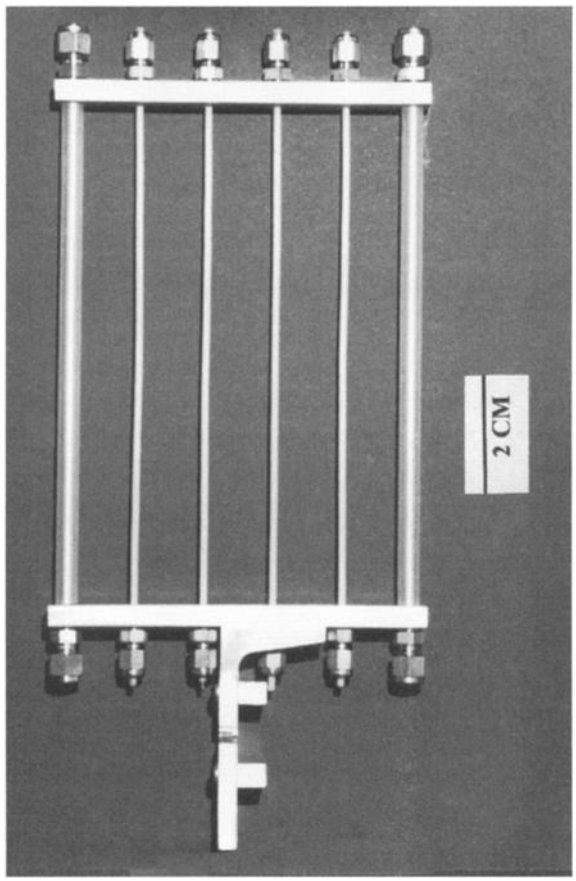

Figure 2. The cloud water impactor used for sampling cloud droplets from the large wind tunnel shown in Figure 1. The two large cylinders of the cloud water impactor have a diameter of 9.5 mm. The four small cylinders have a diameter of 3.2 mm.

using a pitot tube, were varied between 5 and 21 m s^{-1}. Rime sampling intervals ranged between 27 and 210 min. Fluctuations in wind tunnel velocity, resulting both from variability in the ambient wind speed and from ice buildup on the fan blades, were less than ±2 m s^{-1}. The CWI consists of four small (3.2 mm diameter) and two large (9.5 mm diameter) cylinders; each cylinder consists of a stainless steel tube sheathed in Teflon. At the end of each collection interval, the CWI was brought into the cold room (see Figure 1) where the samples were removed from the impactor surfaces and weighed. The delay between sample weighing and chemical processing was never larger than 3 hours. Ice substrate temperatures were inferred from measurements of ambient temperature, tunnel velocity, and riming rate using equations developed by Lozowski et al. [1983]. Substrate temperatures were lower than –3.5°C for all ice samples.

The effective cloud liquid water content (L_e, cm^3 m^{-3}; notation summarized at the end of the manuscript) was calculated using measurements of ice deposit mass (consisting of both impacted droplets and frost formed by vapor deposition), the averaged tunnel velocity, the linear dimensions of the cylinders, and derived values of the vapor deposition to rime mass ratio (*MR*). Our calculation of *MR* is based on the heat flux equations of Lozowski et al. [1983]. Owing to lower droplet collision efficiencies on the 9.5–mm cylinder, the ratio of the two measured L_e, corresponding to concurrent measurements of the deposit mass (corrected for frost deposition), was substantially smaller than unity ($\bar{x}$=0.41, σ=0.16, n=23). Values of the ratio $L_{e,9.5mm}/L_{e,3.2mm}$ and collision efficiency calculations from Langmuir and Blodgett [1946] were used to infer the mass–median droplet radius ($\bar{r}$). It is assumed that the cloud droplets are monodisperse at size $\bar{r}$. The average value of $\bar{r}$ resulting from this calculation was 4.3 μm (σ=1.4 μm, n=23). This average is substantially smaller that the mass–median droplet radius ($\bar{r}$ = 6.5 μm) observed by Rogers et al. [1983] and utilized by SMV. However it is not inconsistent with the climatology presented by Politovich and Vali [1983]. The results presented here were analyzed using a mass–medium droplet radius of 4.3 μm.

Inferred values of droplet collision efficiency, derived from measurements of air velocity, cylinder width, and mass–median droplet radius (4.3 μm), were used to convert L_e to the actual LWC (L, cm^3 m^{-3}). Values of L from the CWI and the CSIRO probe are compared in Figure 3. Overall, the CWI technique overpredicts the actual water content by ~10%. This bias is attributed to increases in droplet collision efficiency due to droplet capture by either frost spikes [Brownscombe and Hallett, 1967] or rime feathers [Keith and Saunders, 1988] that form on the CWI. The overprediction is ~30% if the ice mass due to vapor growth is not accounted for.

Rogers et al. [1983] have published an intercomparison of LWC values obtained from an optical probe and a device similar to the CWS. They reported good agreement between these two measurement techniques, and because of this we have not corrected the CWS LWC values for either droplet collision efficiency or vapor growth effects.

2.3. Gas Sampling

A hydroperoxide monitor identical to the instrument described by Snider and Murphy [1995] was used to measure the gas–phase H_2O_2

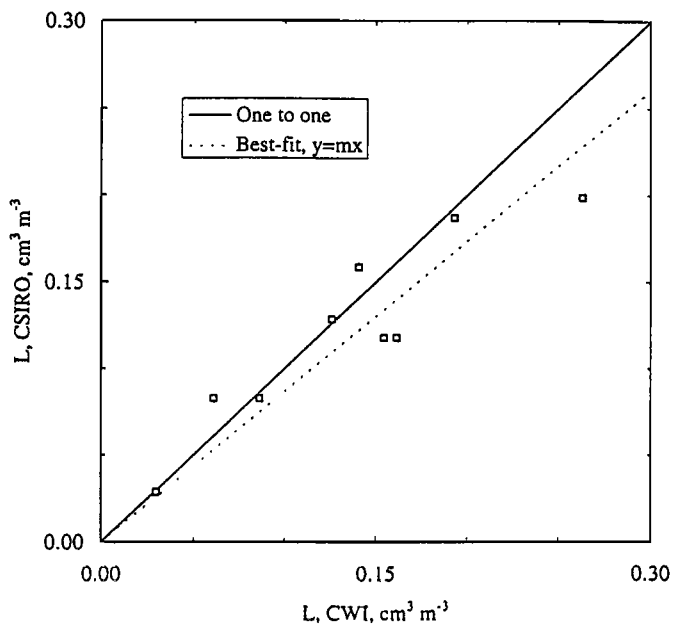

Figure 3. Comparisons of liquid water content based on rime ice collections made with the 3.2–mm cylinder of the cloud water impactor and averages from the CSIRO probe. The dashed line represents the best–fit line corresponding to the equation $y = mx$.

mixing ratio ($\chi_{H_2O_2}$). Characteristics of the sulfur dioxide sensor shown in Figure 1 are described in Snider and Vali (1994). For the experiments conducted in 1991 and 1992, summarized in Table 2, we inferred the concentration of dissolved H_2O_2 in the cloud droplets prior to riming based on the assumption that the hydroperoxide monitor sampled the equilibrium cloud interstitial H_2O_2 mixing ratio. Because a significant fraction of the H_2O_2 is partitioned into the cloud water, it is important to determine if the assumption is invalidated by cloud droplet aspiration or by riming upwind of the sample inlet [Snider and Murphy, 1995]. Both of these processes result in unintentional sampling of the droplet–dissolved H_2O_2, by the hydroperoxide monitor, and underestimation of the H_2O_2 retention efficiency ($\Gamma_{H_2O_2}$). Errors resulting from the latter process are addressed in the Appendix. Here we consider the effects of cloud water aspiration.

A reverse–flow air inlet was used to sample cloud interstitial air from the small wind tunnel shown in Figure 1. This wind tunnel was fabricated using design plans for the Caltech Active Strand Cloud Water Collector (CASCC [Munger et al. 1989]). During normal operation the droplet collection strands were not installed, and the tunnel velocity was 16 m s^{-1}. The reverse–flow sampling strategy contrasts with our previous assessments of $\Gamma_{H_2O_2}$ which were conducted using an inlet which aspirated and internally impacted the cloud droplets (SMV). The reverse–flow inlet tube was fabricated from 10–mm OD borosilicate glass and was heated to approximately 5°C above the ambient temperature by passing a current through an external wrapping of nichrome wire. This inhibited the formation of rime ice on the external surface of the inlet tube. In–cloud testing of the inlet was conducted at the EMO. During some of these tests the inlet was left unheated. These tests showed no evidence of rime buildup inside the inlet tube. Since droplet impaction is expected inside the tube [Huebert et al., 1990], we interpret the absence of rime there to indicate that droplets were not aspirated.

2.4. Measurement of Dissolved O_2 and H_2O_2

Measurements of O_2 in the rime ice (C_{O_2}, mg L^{-1}) were conducted using a vacuum–isolation technique [Huang, 1994]. The collected rime ice was put into a thermostated flask (–10°C), the pressure was lowered to 10 hPa for 3 min, and then O_2–free water was added. The concentration of O_2 in the mixture of melted rime ice and O_2–free water was evaluated using the Winkler method [Carritt and Carpenter, 1966]. A mass balance equation was used to calculate the concentration of O_2 in the rime ice. O_2 losses due to pumping are estimated to be less than 1.8 mg L^{-1} [Huang, 1994]. We illustrate this bias in our plots of the retention efficiency for O_2 (Figure 4).

Hydroperoxides in cloud water consist of H_2O_2 and the organic hydroperoxides [Gunz and Hoffmann, 1990]. The total dissolved concentration of these constituents, symbolized by $[RO_2H]_T$, was determined using the technique of Kok et al. [1986]. So that the fraction of $[RO_2H]_T$ attributable to H_2O_2 could be determined, we divided approximately one in five of the cloud water samples into two aliquots. One was treated with catalase, an enzyme that reacts preferentially with H_2O_2, and subsequently with the reagent p–hydroxyphenylacetic acid (POPAH) [Kok et al., 1986]. The other aliquot was treated directly with the POPAH reagent. The inferred values of $[H_2O_2]$ used in (2) (see section 3.1) were calculated as the product of the measured value of $[RO_2H]_T$ (available for all samples) and the average of the ratio $[H_2O_2]/[RO_2H]_T$. These averages were 1.00±0.04 (n=5), 0.52±0.21 (n=6), 0.66±0.10 (n=10) for the measurements conducted in January 1991, February 1992, and March 1992, respectively. Clearly, this procedure entails possible error in the H_2O_2 content of all samples. In the error analysis we account for the resulting uncertainty by computing a bias based on the assumption that $[H_2O_2]/[RO_2H]_T$ is equal to unity. This correction implies that the measured hydroperoxide concentration corresponds solely to H_2O_2 and therefore provides an upper limit value for the H_2O_2 retention efficiency.

The concentration measurements discussed in the previous paragraphs correspond to the total amounts of O_2 and H_2O_2 retained in the ice. No attempt was made to distinguish between gases located within the ice lattice or inside coexisting phases (i.e., either bubbles or liquid solutions).

3. Calculations

3.1. The Retention Coefficients

$C^*_{O_2}$ and $[H_2O_2]^*$ represent equilibrium concentrations in cloud water predicted by Henry's law. These temperature– and gas partial pressure–dependent concentrations are used to derive the retention efficiencies for O_2 and H_2O_2 in the following manner:

$$\Gamma_{O_2} = \frac{C_{O_2}}{C^*_{O_2}} \tag{1}$$

$$\Gamma_{H_2O_2} = \frac{[H_2O_2]}{[H_2O_2]^*} \tag{2}$$

The retention efficiency represents the relative amount of solute contained in the rime ice relative to that initially in the liquid cloud droplets. This formalism was first introduced by Iribarne and Pyshnov [1990]. Values of $C^*_{O_2}$ were calculated using a Bunsen coefficient (K_{O_2}; Weiss [1970]) evaluated at the ambient temperature (T_a). K_{O_2} is related to the saturated O_2 concentration in the following manner.

$$C^*_{O_2} = \frac{K_{O_2} P_{EMO} \chi_{O_2} M_{O_2}}{V_0 C_2} \tag{3}$$

Here P_{EMO} (0.67×10^5 Pa) is the pressure at EMO, χ_{O_2} is the mole fraction of O_2 in air, M_{O_2} is the molecular weight of O_2, V_0 (22.41 L mol^{-1}) is the volume occupied by a unit mole of ideal gas at standard temperature and pressure (i.e., 273.15 K and 1.01325×10^5 Pa), and C_2 (1.01325×10^5 Pa atm^{-1}) is a unit conversion factor.

Two different techniques, both relying on the Henry's law coefficient for H_2O_2 ($K_{H_2O_2}$), extrapolated to T_a, were used to calculate $[H_2O_2]^*$. For measurements conducted in 1988 and 1989 we used the method discussed in SMV. As a consequence of the larger solubility implied by the revised Henry's law expression of Lind and Kok [1994], the average of $\Gamma_{H_2O_2}$ derived from the 1988–1989 measurements differs by –4% from the average reported in Table 3b of SMV. For the measurements conducted in 1991 and 1992 the following expression was used to calculate $[H_2O_2]^*$.

$$[H_2O_2]^* = K_{H_2O_2} P_{EMO} \chi_{H_2O_2} / C_2 \tag{4}$$

Justification for this approach is discussed in section 2.3 and in the Appendix.

3.2. Characteristic Times

Following the work of SMV we have utilized a modified formula for calculating the droplet impaction time

$$\tau_{im} = \frac{4\varrho_w \bar{r}}{3S^2\beta} \quad (5)$$

This parameter represents the average time interval between impaction events on a specific area of the rime surface. In (5), β is the averaged riming rate per unit area of collection surface, ϱ_w is the density of liquid water, and S is the droplet spreading factor. Values of S were interpolated from the experimental data of Macklin and Payne [1969] and depend on both the droplet impaction velocity (V_{im}, m s^{-1}) and the ice substrate temperature (T_s). The calculated values of S were used to infer the height of the spread droplet (h) [Carras and Macklin, 1975]. SMV evaluated τ_{im} without accounting for droplet spreading, hence the average value of τ_{im} corresponding to the data shown in Figure 6 is a factor of eight smaller than that presented by SMV. This decrease in τ_{im} results because we employ a different value for $\bar{r}$ (see section 2.2) and because most of the derived values of the spreading factor exceed $S = 2$.

Our assessment of the time constant characterizing droplet freezing (τ_2) is based on the theoretical work of Macklin and Payne [1967], which assumes that heat conduction occurs normal to the substrate/droplet interface, and the experimental studies of Carras and Macklin [1975]. We have used the data shown in Figure 6 of Carras and Macklin [1975] to account for heat conduction lateral to the substrate/droplet interface.

Diffusive transport through the freezing or frozen droplet is characterized by a time constant which is expected to vary with the length of the diffusion path and the diffusivity of the solute. If solute diffusion is via liquid [Mulvaney et al., 1988; Mizuno and Hanafusa, 1987], as we have assumed here, then a lower limit value for the solute diffusion time constant is

$$\tau_D = h^2/D \quad (6)$$

Here D is the solute diffusivity within either grain–interstitial or bulk liquid solution. Considerably larger values of τ_D are expected if there is tortuosity associated with the diffusion path, or if diffusion from the frozen droplet is controlled by the much smaller diffusivities associated with diffusion through the crystal lattice. We have ignored potential enhancements to the rate of solute mass transfer due to either droplet shattering [Bari and Hallett, 1974] or the formation of protuberances [Griggs and Choularton, 1983].

The time required to cool both the frozen droplet and the underlying ice substrate back to T_s has been calculated by Macklin and Payne [1967]. A value based on representative conditions at EMO is approximately 0.1 s.

3.3. Criteria for Data Analysis

H_2O_2 can be incorporated into ice either during riming or during uptake into ice formed via the cocondensation of H_2O and H_2O_2 vapors [Sigg and Neftel, 1988]. For a broad range of environmental conditions the latter process produces lower concentrations. Vapor growth during riming can therefore lower the derived values of $\Gamma_{H_2O_2}$. For values of vapor deposition to rime mass ratios greater than 0.1, the effect of H_2O_2 dilution becomes comparable to other experimental uncertainties. Because of this we have eliminated measurements of $\Gamma_{H_2O_2}$ associated with values of $MR > 0.1$ from the analysis. We also use the criteria $[S(IV)]^*/[H_2O_2]^* < 0.1$ and $[Mg^{2+}] < 2.5\ \mu M$ to eliminate low values of H_2O_2 retention which result from reactive depletion of H_2O_2 subsequent to sample collection. These criteria were also utilized by SMV. Because of the much larger partial pressure of O_2 relative to H_2O_2, the ratio $[S(IV)]^*/[O_2]^*$ is always smaller than 0.01, and therefore reactive depletion of dissolved O_2 is not indicated. Hence only the criterion $MR < 0.1$ was used to select values of Γ_{O_2} for the analysis discussed in sections 4 and 5.

4. Results

A summary of the chemical and physical properties of the studied clouds, including averages of gaseous SO_2 and H_2O_2, and properties derived from the measurements, are presented in Table 2. These results are stratified both by year of collection, and therefore by collection technique, and by the criteria discussed in section 3.3. (The subset of values satisfying the selection criteria are shown in parentheses.) The averaged measurements of T_a, L and pH from the 1988–1989 and the 1991–1992 data sets are comparable. Changes in χ_{SO_2}, 0.8 ppbv during 1988–1989 and 0.4 in 1991–1992, correspond to changes in potential H_2O_2 mixing ratio (X), that is, the amount in the gas plus the aqueous phase. This relationship is expected since the in–cloud reaction $SO_2 + H_2O_2$ is an important sink for both trace gases.

Despite the larger values of χ_{SO_2}, averages of $[H_2O_2]$ corresponding to data values selected by the criteria discussed in section 3.3 are larger for the measurements conducted during 1988–1989. Larger $[H_2O_2]$ and smaller X result in larger values of $\Gamma_{H_2O_2}$ during 1988–1989. This is illustrated in Figure 4 where values of $\Gamma_{H_2O_2}$ corresponding to the CWS collections (1988–1989) are indicated by diamonds and the CWI data values (1991–1992) are indicated by triangles. Also shown are error limits corresponding to statistical uncertainties and, for the 1991–1992 data values, upper limit estimates of the retention efficiencies corresponding to the measurement biases discussed in sections 2.3 and 2.4 and in the Appendix. Differences between the H_2O_2 retention measurements obtained using the CWS and those obtained using the CWI typically exceed the uncertainty limits. This observation is consistent with the fact that the 1991 CWS retention efficiency values (indicated by squares) also fall above the 1991–1992 CWI data. Also shown in Figure 4 are retention efficiencies for O_2 (indicated by circles), the corresponding statistical uncertainties, and upper limit error estimates based on the assumption of a 1.8 mg L^{-1} underestimate in C_{O_2} (see section 2.4).

5. Discussion

Rime ice collections with the CWI use droplet impaction velocities (V_{im}) which are considerably smaller than those for the CWS. Smaller values of V_{im} occur because both the large and the small cylinders of the CWI are broader than the width of the CWS and because the air velocity in the large wind tunnel was lower than the tangential velocity of the CWS (Table 2). Positive correlations between retention and V_{im} are seen for both O_2 and H_2O_2 in Figure 5.

Also plotted are the domain of the CWS H_2O_2 retention values, defined by two standard deviations in both $\Gamma_{H_2O_2}$ and V_{im}, and the extreme CWS values. The apparent discontinuity in $\Gamma_{H_2O_2}$ at V_{im}

Table 2. Comparison of Measurements From 1988–1989 and 1991–1992

	T_a, °C	L, $cm^3\ m^{-3}$	pH	χ_{SO2}, ppbv	X, ppbv	$[H_2O_2]$, μM	$[S(IV)]^*/[H_2O_2]^*$	V, $m\ s^{-1}$	Γ_{H2O2}	Γ_{O2}
					Wintertime 1988–1989; Cloud Water Sampler (CWS)					
$\bar{x}$	−11 (−7) [a]	0.13 (0.19) [a,b]	4.6 (4.5) [a]	0.8 (0.4) [a,c]	0.3 (0.6) [a,c]	14 (19) [a]	0.74 (0.02) [a,d]	19 (19) [a,c,e]	0.20 (0.23) [a]	na [f]
σ	5 (2)	0.09 (0.08)	0.6 (0.4)	0.5 (0.3)	0.3 (0.3)	10 (9)	2.51 (0.02)	1 (1)	0.09 (0.06)	na
max	−4 (−4)	0.41 (0.41)	6.2 (5.4)	3.0 (1.1)	1.4 (1.4)	34 (34)	17.09 (0.06)	24 (24)	0.39 (0.36)	na
min	−24 (−13)	0.01 (0.04)	3.6 (4.0)	>.0 (>.0)	>.0 (0.13)	1 (3)	>.00 (>.00)	13 (13)	0.01 (0.06)	na
n	87 (31)	87 (31)	87 (31)	87 (31)	87 (31)	87 (31)	87 (31)	87 (31)	87 (31)	na
					Wintertime 1991–1992; Cloud Water Impactor (CWI)					
$\bar{x}$	−9 (−10) [a]	0.15 (0.23) [a,b]	4.4 (4.5) [a]	0.4 (0.5) [a,c]	0.8 (1.1) [a,c]	13 (7) [a]	0.01 (0.01) [a,d]	17 (17) [a,c,e]	0.07 (0.05) [a]	0.25 (0.32) [g]
σ	1 (1)	0.12 (0.08)	0.5 (0.4)	0.4 (0.5)	0.5 (0.4)	10 (5)	0.01 (0.01)	4 (3)	0.04 (0.02)	0.13 (0.10)
max	−6 (−8)	0.54 (0.41)	5.3 (5.2)	1.6 (1.6)	2.0 (2.0)	40 (16)	0.05 (0.04)	21 (20)	0.16 (0.10)	0.52 (0.52)
min	−14 (−11)	>0.00 (0.12)	3.3 (3.9)	0.1 (0.1)	0.1 (0.4)	1 (1)	>.00 (>.00)	5 (9)	0.01 (0.01)	0.03 (0.17)
n	59 (23)	59 (23)	49 (19)	59 (22)	59 (14)	50 (14)	48 (14)	59 (23)	50 (14)	22 (12)

[a] Values in parentheses correspond to the subset of samples satisfying the criteria: $[S(IV)]^*/[H_2O_2]^*<0.1$, $MR<0.1$, and $[Mg^{2+}] < 2.5$ μM.

[b] The 1991–1992 values of the actual LWC were derived by correcting both for ice sample mass due to vapor growth and droplet impaction inefficiency. Neither of these corrections was applied to the 1988–1989 data. See text for details.

[c] χ_{SO_2}, X, and V were obtained by averaging continuous measurements over the rime collection intervals.

[d] This is the ratio of the equilibrium concentrations of S(IV) and H_2O_2 based on the measurements of LWC, SO_2 and H_2O_2 mixing ratios, solution pH, and temperature (see SMV).

[e] Summarized here are both CWS average tangential velocity and standard deviation (1988–1989 samples) and average wind tunnel velocity and standard deviation. Statistics for the CWS are sample–volume weighted averages.

[f] Abbreviation na, not available.

[g] Values in parentheses correspond to the subset of samples satisfying the criterion $MR<0.1$ (see text for details).

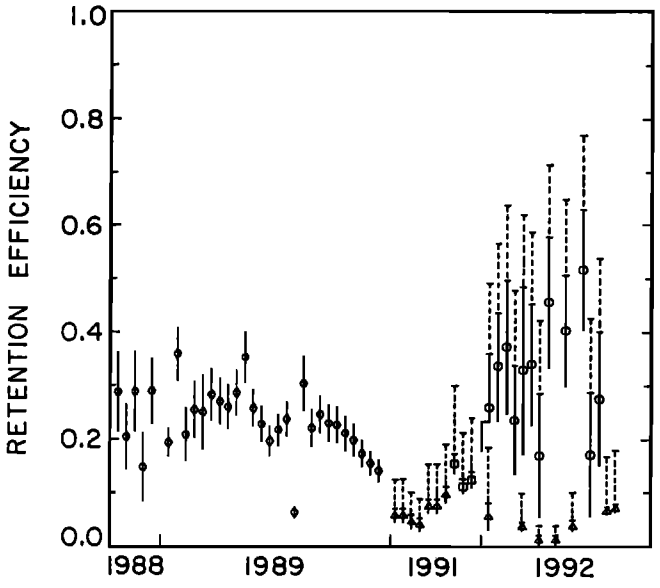

Figure 4. Values of H_2O_2 retention ($\Gamma_{H_2O_2}$; diamonds, triangles, and squares), and O_2 retention (Γ_{O_2}; circles) selected by the criteria discussed in section 3.3. Samples from 1988 and 1989 (diamonds) were collected using the cloud water sampler. The 1991 samples, collected using the cloud water sampler, are symbolized by squares. All other samples were collected using the cloud water impactor. Statistical uncertainties are indicated by solid vertical lines. The top of the dashed vertical line segments indicate upper limit error estimates in the 1991/1992 measurements of both $\Gamma_{H_2O_2}$ and Γ_{O_2}. O_2 losses during sample processing, possibly as large as 1.8 mg L^{-1} [Huang, 1994], were used to infer the upper limit values for Γ_{O_2}. For H_2O_2, the upper limit estimate is based on two assumptions: $[H_2O_2] = [RO_2H]_T$ (see section 2.4) and (8) (see Appendix).

~15 m s^{-1} may reflect differences in the techniques used to sample gaseous H_2O_2 or may represent an actual nonlinearity in H_2O_2 retention at this particular impact velocity. The fact that there were three 1991 samples (squares in Figure 4), which were collected using the CWS and which exhibited retention values larger than all the measurements derived using the CWI, argues in favor of the latter hypothesis.

At a substrate temperature of –11°C, the droplet spreading factor (S) increases from 1.8 to 2.3 for a 2.5 to 15 m s^{-1} change in V_{im} [Macklin and Payne, 1969]. Since riming rate (β) is also expected to increase with V_{im} (assuming constant LWC), (5) predicts that τ_{im} and V_{im} should vary inversely. The correlation between τ_{im} and V_{im} for the CWI data set is consistent with this expectation (regression coefficient = –0.9, n = 23, probability of accidental correlation (p) < 0.0001). The inverse correlation between retention and τ_{im} (Figure 6) is therefore consistent with the τ_{im}/V_{im} relationship and the results plotted in Figure 5.

The inverse correlations shown in Figure 6 suggest a link between O_2 and H_2O_2 retention and the rate of droplet impaction. SMV discuss explanations for this and propose a retention model in which gas volatilization from frozen droplets residing on the ice surface is inhibited by subsequent impaction events. One way that this may occur is that subsequent impaction events increase the distance required for solute diffusion. In the discussion that follows we utilize observed values of β, corresponding to rime ice collection made with the 3.2–mm cylinder of the CWI (0.0008 to 0.0028 kg m^{-2} s^{-1}), in a further analysis of the proposed retention model.

The summary of characteristic times shown in Figure 7 demonstrates that the values of τ_D (evaluated at D=7x10^{-10} m^2 s^{-1}) and τ_2 differ by a factor of forty. This difference implies that only a small fraction of the solute load can volatilize during the freezing process, hence a large fraction of the total must be lost via a mechanism involving mass transport through the frozen droplet. Two effects produced by the freezing process establish conditions which enhance solute volatilization subsequent to freezing. The first of these is the increased temperature, and lowered gas solubility, associated with the release of the latent heat of fusion. In this regard it is important to point out that approximately 0.1 s is required to dissipate the thermal perturbation caused by a single droplet freezing event [Macklin and Payne, 1967]. The other effect is the exclusion of solute from the lattice and its accumulation within grain–interstitial inclusions within the freezing droplet. Both effects increase the chemical potential of solute relative to that in the gas phase and therefore establish a driving force for either solute volatilization or bubble nucleation. The calculated droplet freezing rates (i.e., h/τ_2) for our CWI experiments (0.009 to 0.017 m s^{-1}) are comparable to those found by Bari and Hallett [1974] in their study of the impaction of 3–mm water drops onto a metal substrate at –150°C. Bari and Hallett found that warming the central portions of the frozen drops to –10°C resulted in the formation of bubbles along grain boundaries. This observation implies that a significant fraction of the solute N_2

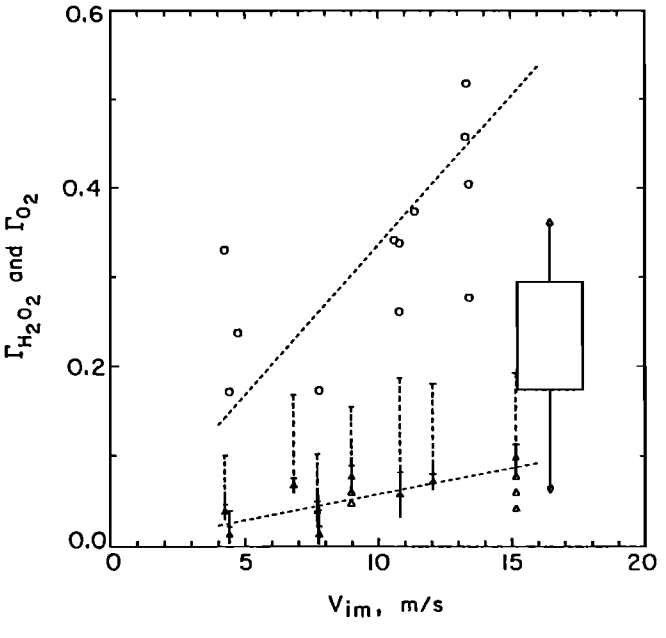

Figure 5. Retention efficiency plotted as a function of the droplet impact velocity. For clarity, error bars are not shown for the O_2 retention measurements (circles) or for five of the H_2O_2 measurements. The 1988–1989 H_2O_2 measurements are represented by the extreme values (diamonds) and by a box centered at the averages of droplet impaction velocity and the retention efficiency. The width and height of the box are equivalent to two standard deviations. The dashed lines are fits of the form $y = mx$. Only the cloud water impactor data were used to infer the $\Gamma_{H_2O_2}$ best–fit line.

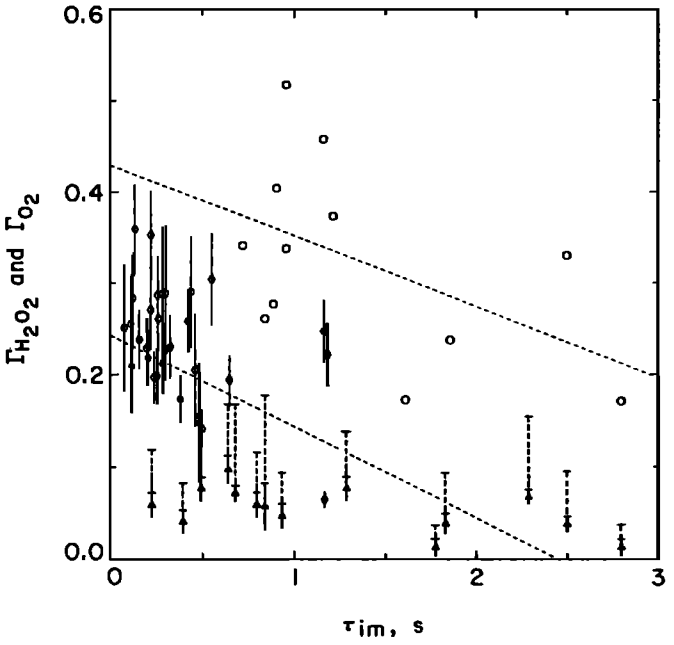

Figure 6. O_2 (circles) and H_2O_2 (diamonds and triangles) retention efficiencies versus droplet impact time. Uncertainties are shown as in Figure 4 but for only the H_2O_2 data points. The dashed lines are fits of the form $y = mx + b$. Both the cloud water impactor and the cloud water sampler data were used to infer the best–fit line for the H_2O_2 measurements.

and O_2 can be concentrated within the grain–interstitial regions during freezing. We conclude from this work, and from the fact the freezing rates were comparable both in the Bari and Hallett experiments and in our riming study, that appreciable solute exclusion also occurs during freezing associated with riming. Furthermore, we contend that this grain–interstitial solute can readily diffuse to the ice/air interface. Support for the latter assumption comes from the work of Diehl et al. [1995]. These investigators have shown that diffusion of both HNO_3 and HCl in ice ($T = -19^0$C) is consistent with a diffusivity that ranges between 0.5×10^{-12} and 1.1×10^{-12} m^2 s^{-1}. In Figure 7 we have plotted values of τ_D calculated using (6) and an assumed value of D equal to 10^{-12} m^2 s^{-1}. Here it is apparent that the characteristic time for solute mass loss via diffusion ($\tau_D \sim 3$ s at $\bar{r} = 4.3$ μm) is comparable to the time interval separating droplet impaction events. This comparison, and the experimental results which show smaller values of retention at larger values of τ_{im} (Figure 6), are both consistent with our hypothesis that a significant amount of solute volatilization occurs subsequent to freezing.

The retention measurements shown in Figures 5 and 6 allow us to speculate about the extent of gaseous solute retention during collisional interactions between graupel and supercooled droplets. Based on the data presented in Figure 5 we conclude that retention of both O_2 and H_2O_2 increases with graupel fall speed. It should also be noted that most graupel particles intercept droplets at impaction velocities considerably smaller than 15 m s^{-1}. Hence the $\Gamma_{H_2O_2}$ values published by SMV appear to define an upper limit estimate of the H_2O_2 retention efficiency during precipitation formation via riming. It should also be recognized that the retention efficiency measurements reported in this paper, and by SMV, were conducted in wintertime clouds containing LWC values roughly an order of magnitude smaller than that observed in convective clouds. By the same reasoning, the mass–median droplet radius for convective clouds, particularly precipitating convective clouds, is also larger than that observed during winter at Elk Mountain. Although these differences make extrapolations rather uncertain, we contend that the best–fit relationships shown in Figure 6 provide a useful guide for estimating trace gas retention during accretional growth. Assuming a graupel diameter of 1 mm, and using representative values for $\bar{r}$, β, T_s, and V_{im}, computed values of τ_{im} (equation 5) range between 2 and 9 s. Values of τ_{im} equal to 2 s correspond to conditions in precipitating convective clouds, and values of τ_{im} equal to 9 s correspond to wintertime orographic clouds. This calculation indicates that the experimental data shown in Figure 6 can be used to predict both Γ_{O_2} and $\Gamma_{H_2O_2}$ for the former but not for the latter environment. It should also be pointed out that all of our measurements correspond to ice substrate temperatures colder than –3.5°C. Hence inferences based on the retention/τ_{im} relationships in Figure 6 should only be applied to dry growth conditions.

6. Conclusions

The averaged value of $\Gamma_{H_2O_2}$ is 0.05 when collections are made on a set of cylindrical collection rods, the CWI. The average increases to 0.23 for samples collected using a rotated collector, the CWS (SMV). The CWI cylinders (3.2 and 9.5 mm) are broader than the CWS impaction ribbons (0.5 mm). Also, the CWI was used to sample

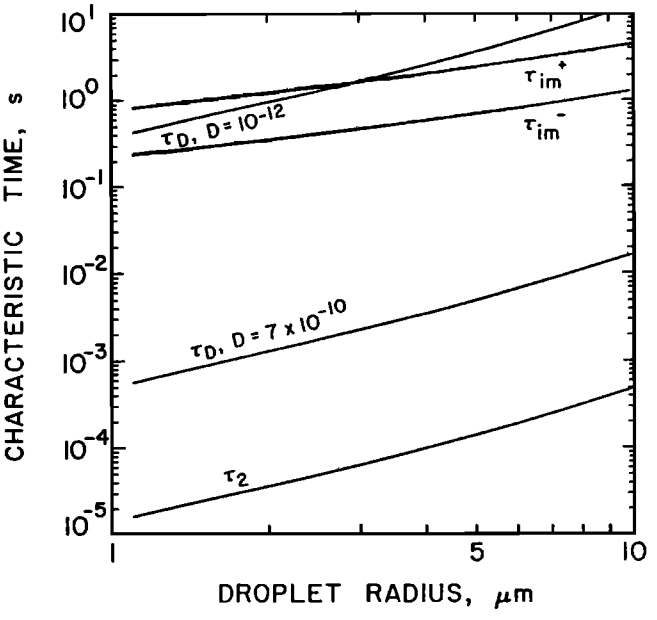

Figure 7. Calculations of the characteristic times for droplet freezing (τ_2), solute diffusion (τ_D, lower curve for liquid–phase diffusion, upper curve based on values of solute diffusivity in ice published by Diehl et al. [1995]), and droplet impaction (τ_{im}) assuming collection by a 3.2 mm cylinder and averaged conditions from Table 2. Droplet impact times τ_{im}^+ and τ_{im}^- correspond to the maximum and minimum values of riming rate observed during this study. Droplets smaller than 1.1 μm are not collected by the cloud water impactor. Liquid–phase solute diffusivity is based on the temperature extrapolations discussed by Schwartz [1986].

cloud droplets from a wind tunnel operated at velocities equal to or smaller than the tangential velocity of the CWS. These field measurements of $\Gamma_{H_2O_2}$ are considerably smaller than the laboratory measurements of Iribarne and Pyshnov [1990]. The average retention efficiency for O_2, derived from measurements made using the CWI, was 0.32.

As is discussed in the Appendix, direct measurements of H_2O_2 volatilization were also conducted. These experiments suggest that liquid cloud droplets contain an amount of H_2O_2 consistent with the temperature–extrapolated prediction of Henry's law. Hence the disparity between our field measurements of $\Gamma_{H_2O_2}$ and the laboratory measurements conducted by Iribarne and Pyshnov [1990] is not due to subsaturated H_2O_2 concentrations in the cloud droplets at Elk Mountain.

Laboratory measurements of the ice/solution distribution coefficient for O_2 and H_2O_2 are reported by Körber [1988] and Sigg and Neftel [1988], respectively. From these studies it is anticipated that a larger fraction of H_2O_2 is rejected into the grain–interstitial liquid during freezing compared to O_2. As a consequence, it is expected that a larger fraction of H_2O_2, in comparison with O_2, is available for loss via diffusive mass transfer through grain–interstitial liquid inclusions. This prediction is consistent with our conceptual model and with the fact that $\Gamma_{O_2} > \Gamma_{H_2O_2}$. It should be emphasized that solute retention during riming is controlled by mass transport and not by the equilibrium properties of the gas/water system. If equilibrium conditions were maintained during riming then the retention efficiency could be predicted from ice/solution distribution coefficients evaluated at 273 K (0.05 for O_2 [Körber, 1988] and 0.014 for H_2O_2 [Sigg and Neftel, 1988]) and enthalpy data corresponding to the Henry's law solubility of the gas. This is clearly not the case. Even so, the thermodynamic data establish lower limit values for the retention efficiency. It is expected that future investigators of the retention process will benefit from an examination of equilibrium solute partitioning at the solid/solution interface and also from a consideration of our proposed solute volatilization mechanism.

Appendix: Cloud–interstitial H_2O_2

The H_2O_2 retention efficiency values based on (2) and (4) are predicated on the assumption that the reverse–flow inlet samples an amount of cloud interstitial H_2O_2 consistent with equilibrium theory. Two processes are expected to produce enhancements of the H_2O_2 mixing ratio relative to that anticipated for equilibrium sampling and may therefore lead to underestimation of the H_2O_2 retention efficiency. First, there is the issue of droplet aspiration (section 2.3). The second process is H_2O_2 volatilization due to riming on surfaces upwind of the inlet. Here we examine the degree to which upstream riming biases the H_2O_2 retention measurement. This assessment was conducted by comparing observations of H_2O_2 inside clouds, made using the reverse–flow inlet (Figure 1), and theoretical predictions of the gas/aqueous partitioning of H_2O_2.

The comparisons summarized in the top rows of Table 3 correspond to transitions from in–cloud to clear–air conditions. Here X is the potential H_2O_2 mixing ratio corresponding to measurements of gaseous H_2O_2 made in clear–air, and the fraction $R(T_a, L)$ represents the cloud–water–dissolved to cloud–interstitial H_2O_2 ratio. Assuming equilibrium conditions, $R(T_a, L)$ is given by

$$R(T_a, L) = K_{H_2O_2} L R_u T_a C_1 / C_2 \quad (7)$$

where T_a is the ambient temperature, R_u is the universal gas constant, $K_{H_2O_2}$ is the Henry's Law constant for H_2O_2 [Lind and Kok, 1994], and C_1 (10^{-3} L cm^{-3}) and C_2 (1.01325×10^5 Pa atm^{-1}) are unit conversion factors. During the experiment conducted on January 17, 1992, there was a large difference (i.e., +140%) between the observed and predicted cloud interstitial H_2O_2 mixing ratio. This positive bias is indicated by the value of Δ in the eighth column of Table 3. On February 13, 1992, the values of both $R(T_a, L)$ and Δ were considerably smaller. Assuming there was no change in air mass associated with the in–cloud to clear–air transition, the measurements summarized in the first two rows of Table 3 indicate that there is a positive bias associated with the measurements of cloud interstitial H_2O_2. The aircraft measurements of Snider and Murphy [1995] are consistent with this conclusion. We account for this bias by correcting the measured values of $\chi_{H_2O_2}$ to a lower limit estimate ($\chi'_{H_2O_2}$) using the equation

$$\chi'_{H_2O_2} = \frac{\chi_{H_2O_2}}{0.2 \cdot R(T_a, L) + 1} \quad (8)$$

Here it is assumed that Δ is equal to $0.2 \cdot R(T_a, L)$. This approach is conservative since it overestimates the observed values of Δ in Table 3. We use this technique to predict the upper limit values of $\Gamma_{H_2O_2}$ shown in Figures 4, 5, and 6.

Table 3. Measurements of Gaseous H_2O_2

Date	T_a, °C	L_e, cm^3 m^{-3}	L, cm^3 m^{-3}	X, ppbv	χ_{H2O2}, ppbv	$R(T_a, L)$	Δ
			In–cloud and Clear–air Measurements				
Jan. 17, 1992	−11.4	0.109	0.237 [a]	0.12	0.03	9.8	1.4 [b]
Feb. 13, 1992	−5.5	0.033	0.045 [a]	0.63	0.34	1.13	0.1 [b]
			In–cloud and Riming–perturbed Measurements				
Feb. 15, 1992 – 1	−8.4	0.039	0.054 [a]	0.84	0.29	1.73	−0.1 (0.1) [b, c]
Feb. 15, 1992 – 2	−8.5	0.041	0.057 [a]	0.98	0.25	1.83	−0.3 (−0.1) [b, c]
Feb. 15, 1992 – 3	−8.1	0.046	0.064 [a]	0.90	0.26	1.99	−0.1 (0.1) [b, c]

[a] The actual LWC, was calculated as $L = L_e/F$, where F is the collision efficiency assuming a mass–median droplet radius of 4.3 μm.

[b] Departures (Δ) between measurement and equilibrium theory are given by $\Delta = (\chi_{H_2O_2} - X/(R(T_a, L) + 1))/(X/(R(T_a, L) + 1))$. For the experiments conducted on January 17, 1992 and February 13, 1992, X was taken to be the value of the hydrogen peroxide mixing ratio observed in clear air. For the February 15, 1992 experiments, (9) was used to calculate X. This calculation was based on an inferred droplet collision efficiency ($F = 0.81$) and an assumed fraction of the inlet masked by the strands ($f = 0.86$, [Munger et al., 1989]).

[c] Values of Δ shown in parentheses were calculated using (9) and the values $f = 1$ and $F = 1$. See text for details.

The February 15, 1992, measurements of in-cloud H_2O_2 were conducted by intentionally riming cloud droplets upstream of the reverse-flow inlet. Shown in Figure 8 are measurements of $\chi_{H_2O_2}$, T_a, and L. Here the short-dashed vertical lines preceding the increase in $\chi_{H_2O_2}$ indicate when the droplet collection strands were inserted into the wind tunnel. These lines also define the end of the averaging intervals (5 min) used to characterize H_2O_2 measurements unperturbed by riming (sixth column of Table 3). Also shown in Figure 8 (long-dashed vertical lines) are the ends of the averaging intervals for data perturbed by riming. The values of T_a, L, and the H_2O_2 mixing ratio perturbed by riming ($\tilde{X}$) were evaluated over this five min interval. This averaging interval includes the $\chi_{H_2O_2}$ maximum which occurs prior to the time we removed the droplet collection strands.

For the reverse-flow inlet tests conducted on February 15, 1992, we have based the comparison of cloud interstitial and riming-perturbed H_2O_2 measurements on a mass balance over that observed in the gas phase ($\tilde{X}$) and over that assumed to be volatilized from the cloud droplets. The potential H_2O_2 mixing ratio which characterizes this mass balance is given by

$$X = \frac{\tilde{X} \cdot (R(T_a, L) + 1)}{1 + fFR(T_a, L)(1 - \Gamma_{H_2O_2})} \quad (9)$$

where f is the fraction of small wind tunnel opening masked by the collection strands (i.e., 0.86 [Munger et al., 1989]). The second term in the denominator of (9) accounts for solute H_2O_2 volatilized during riming [Snider and Murphy, 1995]. Values of Δ from February 15, 1992, are smaller than that observed during the in-cloud/clear-air tests (i.e., January 17 and February 13, 1992). Using the value $fF = 1$, that is, assuming that all droplets entering the small wind tunnel are impacted as opposed to the predicted fraction $fF = 0.68$, produces better agreement with the values of Δ obtained from the in-cloud/clear-air tests. The values of Δ based on the assumption $fF = 1$ are shown in parentheses in Table 3. This correction is justified since riming on the collection strands was observed to increase f and because simultaneous increases in F, due to the formation of rime feathers and frost, are also expected. Our interpretation of the observations shown in Figure 8, and the correction we have applied in Table 3, are also consistent with the fact that the time constant characterizing the response of the hydroperoxide monitor subsequent to the insertion of the collection strands (~10 min) is commensurate with the time interval required for icing to double the mass of the collection strands but not with the much shorter response time of the hydroperoxide monitor (i.e., ~20 s [Snider and Murphy, 1995]). Mechanical loss of the rime ice subsequent to the $\chi_{H_2O_2}$ maximum, and the associated decreases in both f and F, are thought to explain the slow rate of $\chi_{H_2O_2}$ decrease observed prior to the much more pronounced decrease in $\chi_{H_2O_2}$ associated with the removal of the collection strands. Furthermore, we attribute the slower than expected response to conditions unperturbed by the collection grid (here the $1/e$ time constant is ~3 min) to the reversible desorption of H_2O_2 from the inner walls of the Teflon sample tube. Cocondensation of a H_2O_2/H_2O mixture [Conklin et al., 1993] is expected since air sampled downwind of the collection strands is characterized by a frost point temperature larger than the ambient temperature.

The three $\chi_{H_2O_2}$ maxima, shown in Figure 8, indicate that appreciable H_2O_2 volatilization results from rime forming on the droplet impaction grid located upwind of the sample inlet. H_2O_2 mass balance calculations for the experiments conducted on February 15, 1992, shown in Table 3, quantify this assertion. Our successful application of this experimental approach points to an alternate method for evaluating the retention efficiencies of compounds that are characterized by Henry's law coefficients larger than ~10^5 M atm^{-1}.

Notation

C_1	unit conversion factor (10^{-3} L cm^{-3}).
C_2	unit conversion factor (1.01325×10^5 Pa atm^{-1}).
f	masked fraction of small wind tunnel opening.
F	droplet collision efficiency.
h	thickness of the impacted droplet, cm or m.
$[H_2O_2]$	H_2O_2 concentration in melted rime, μM or M.
$[H_2O_2]^*$	equilibrium H_2O_2 concentration, μM or M.
K_{O_2}	Bunsen coefficient, L atm^{-1}.

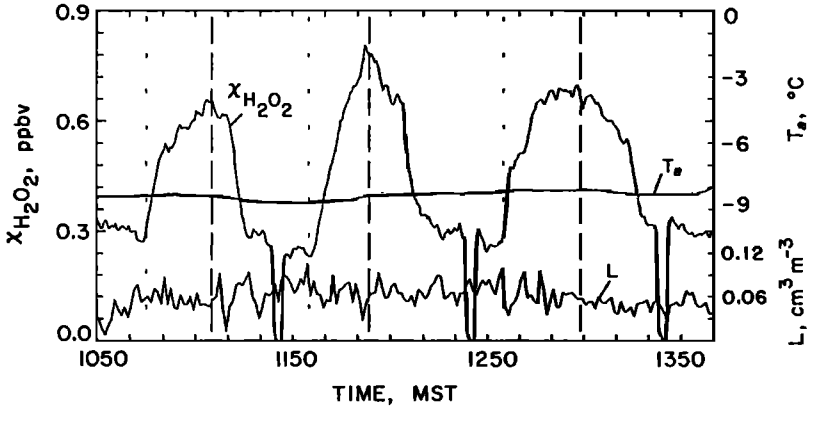

Figure 8. Time series plots of gas-phase H_2O_2 mixing ratio, ambient temperature, and cloud water content from February 15, 1992. Three-minute zeroing intervals for H_2O_2 are seen to bracket increases in gaseous H_2O_2 resulting from the insertion of droplet collection strands into the front of the small wind tunnel. Vertical lines with short dashes indicate the end of 5-min averaging intervals and when the droplet collection strands were installed. Vertical lines with long dashes indicate the end of 5-min averaging intervals for the H_2O_2 mixing ratio perturbed by riming upwind of the reverse-facing inlet.

$K_{H_2O_2}$	Henry's law coefficient, **M** atm^{-1}.
L	actual cloud liquid water content, $cm^3\ m^{-3}$.
L_e	effective cloud liquid water content, $cm^3\ m^{-3}$.
M_{O_2}	molecular weight of O_2, gm mol^{-1}.
MR	vapor deposition to rime mass ratio.
P_{EMO}	pressure at EMO, hPa or Pa.
p	probability of accidental correlation (t–test).
$\bar{r}$	mass–median droplet radius, μm or m.
$[RO_2H]_T$	hydroperoxide concentration in melted rime, μM or **M**.
$R(T_a, L)$	cloud water to gas–phase H_2O_2 equilibrium ratio.
R_u	universal gas constant, 8.314 Pa $m^3\ mol^{-1}\ K^{-1}$.
S	droplet spreading factor.
T_a	ambient temperature, °C or K.
T_s	rime substrate temperature, °C or K.
V_0	22.41 L mol^{-1}.
V	wind tunnel or collector velocity, m s^{-1}.
V_{im}	droplet impaction velocity, m s^{-1}.
ϱ_w	density of liquid water.
$\chi_{H_2O_2}$	gas–phase H_2O_2 mixing ratio.
X	potential H_2O_2 mixing ratio.
$\bar{X}$	H_2O_2 mixing ratio perturbed by riming.
χ_{O_2}	gas–phase O_2 mixing ratio.
χ_{SO_2}	gas–phase SO_2 mixing ratio.
$\Gamma_{H_2O_2}$	H_2O_2 retention efficiency.
Γ_{O_2}	O_2 retention efficiency.
Δ	measured to equilibrium difference in $\chi_{H_2O_2}$.
τ_{im}	droplet impaction time, s.
τ_D	characteristic time for solute diffusion, s.
τ_2	droplet freezing time, s.
β	riming rate, kg $m^{-2}\ s^{-1}$.

Acknowledgments. This work was supported by National Science Foundation grants ATM-9012805 and ATM-9314358.

References

Bari, S. A., and J. Hallett, Nucleation and growth of bubbles at an ice–water interface, *J. Glaciol., 13,* 489–520, 1974.

Brownscombe, J. L. and J. Hallett, Experimental and field studies of precipitation particles formed by the freezing of supercooled water, *Q. J. R. Meteorol. Soc., 93,* 455–473, 1967.

Carras, J. N. and W. C. Macklin, Air bubbles in accreted ice, *Q. J. R. Meteorol. Soc., 101,* 127–146, 1975.

Carritt, D. E., and J. H. Carpenter, Comparison and evaluation of currently employed modifications of the Winkler method for determining dissolved oxygen in seawater; a NASCO report, *J. Mar. Res., 24,* 286–318, 1966.

Cho, H. R., M. Neiwiadomski, J. V. Iribarne, and O. Melo, A model of the effect of cumulus clouds on the redistribution and transformation of pollutants, *J. Geophys. Res., 94,* 12895–12910, 1989.

Conklin, M. H., A. Sigg, A. Neftel, and R. C. Bales, Atmosphere–snow transfer function for H_2O_2: Microphysical considerations, *J. Geophys. Res., 98,* 18367–18376, 1993.

Diehl, K., S. K. Mitra, and H. R. Pruppacher, A laboratory study of the uptake of HNO_3 and HCl vapor by snow crystals and ice spheres at temperatures between 0 and –40 °C, *Atmos. Environ., 29,* 975–981, 1995.

Griggs, D. J., and T. W. Choularton, Freezing modes of riming droplets with application to ice splinter production, *Q. J. R. Meteorol. Soc., 109,* 243–253, 1983.

Gunz, D. W., and M. R. Hoffmann, Atmospheric chemistry of peroxides: A review, *Atmos. Environ., 24A,* 1601–1633, 1990.

Huang, J., Measurements of O_2 and H_2O_2 retention in rime ice, M.S. Thesis, University of Wyoming, Laramie, 1994.

Huebert, B. J., G. Lee, and W. L. Warren, Airborne aerosol inlet passing efficiency measurement, *J. Geophys. Res., 95,* 16369–16381, 1990.

Iribarne, J. V., and T. Pyshnov, The effect of freezing on the composition of supercooled droplets, I, Retention of HCl, HNO_3, NH_3 and H_2O_2, *Atmos. Environ., 24A,* 383–387, 1990.

Iribarne, J. V., T. Pyshnov, and B. Naik, The effect of freezing on the composition of supercooled droplets, II, Retention of S(IV), *Atmos. Environ., 24A,* 389–398, 1990.

Keith, W. D., and C. P. R. Saunders, The collection efficiency of a rime–covered target for water droplets, *Atmos. Res., 22,* 105–123, 1988.

King, W. D., D. A. Parkin, and R. J. Handsworth, A hot–wire liquid water device having fully calculable response characteristics, *J. Appl. Meteor., 17,* 1809–1813, 1978.

Kok, G. L., K. Thompson, A. L. Lazrus, and S. E. McLaren, Derivatization technique for the determination of peroxides in precipitation, *Anal. Chem., 58,* 1192–1194, 1986.

Körber, C., Phenomena at the advancing ice–liquid interface: Solutes, particles and biological cells, *Q. Rev. Biophys., 21,* 229–298, 1988.

Lamb, D., and R. Blumenstein, Measurement of the entrapment of sulfur dioxide by rime ice, *Atmos. Environ., 21,* 1765–1772, 1987.

Langmuir, I., and K. B. Blodgett, Mathematical investigation of water droplet trajectories, *U.S. Air Force Tech. Rep. 5418,* U.S. Army Air Forces, Dayton, OH, 1946.

Lind, J. A., and G. L. Kok, Correction to "Henry's law determination for aqueous solutions of hydrogen peroxide, methylhydroperoxide, and peroxyacetic acid" by John A. Lind and Gregory L. Kok, *J. Geophys. Res., 99,* 21119, 1994.

Lozowski, E. P., J. R. Stallabrass, and P. F. Hearty, The icing of an unheated, nonrotating cylinder, I, A simulation model, *J. Clim. Appl. Meteorol.., 22,* 2053–2062, 1983.

Macklin, W. C., and G. S. Payne, A theoretical study of the ice accretion process, *Q. J. R. Meteorol. Soc., 93,* 195–213, 1967.

Macklin, W. C., and G. S. Payne, The spreading of accreted droplets, *Q. J. R. Meteorol. Soc., 95,* 724–730, 1969.

Mizuno, Y., and N. Hanafusa, Studies of surface properties of ice using nuclear magnetic resonance, *J. Phys.,* C1, 511–519, 1987.

Mulvaney, R., E. W. Wolff, and K. Oates, Sulfuric acid at grain boundaries in Antarctic ice, *Nature, 331,* 247–249, 1988.

Munger, J. W., J. Collett, B. Daube, and M. R. Hoffmann, Chemical composition of coastal stratus clouds: Dependence on droplet size and distance from the coast, *Atmos. Environ., 23,* 2305–2320, 1989.

Politovich, M .K., and G. Vali., Observations of liquid water in orographic clouds over Elk Mountain, *J. Atmos. Sci., 40,* 1300–1312, 1983.

Rogers, D. C., D. Baumgardner and G. Vali, Determination of supercooled liquid water content by measuring rime rate, *J. Clim. Appl. Meteorol., 22,* 153–162, 1983.

Schwartz, S. E., Mass–transport considerations pertinent to aqueous phase reactions of gases in liquid–water clouds, in *Chemistry of Multiphase Systems,* edited by W. Jaeschke, pp. 415–472, Springer–Verlag, New York, 1986.

Sigg, A., and A. Neftel, Seasonal variations in hydrogen peroxide in polar ice cores, *Ann. Glaciol., 10,* 157–162, 1988.

Snider, J. R., and T. Murphy, Airborne hydrogen peroxide measurements in supercooled clouds, *J. Geophys. Res., 100,* 23039–23050, 1995.

Snider, J. R., and G. Vali, Sulfur dioxide oxidation in winter orographic clouds, *J. Geophys. Res., 99,* 18713–18733, 1994.

Snider, J. R., D. C. Montague, and G. Vali, Hydrogen peroxide retention in rime ice, *J. Geophys. Res., 97,* 7569–7578, 1992.

Weiss, R. F., The solubility of nitrogen, oxygen and argon in water and seawater, *Deep Sea Res., 17,* 721–735, 1970.

J. Huang and J.R. Snider, Department of Atmospheric Science, University of Wyoming, P.O. Box 3038, Laramie, WY 82071-3038. (e-mail snider@grizzly.uwyo.edu)

(Received May 2, 1996; revised September 26, 1997; accepted September 30, 1997.)